International Journal of Greenhouse Gas Control 64 (2017) 152–162

Contents lists available at ScienceDirect

International Journal of Greenhouse Gas Control

journal homepage: www.elsevier.com/locate/ijggc

X-ray CT and multiphase flow characterization of a 'bio-grouted' sandstone core: The effect of dissolution on seal longevity

James M. Minto[a,*], Ferdinand F. Hingerl[b], Sally M. Benson[c], Rebecca J. Lunn[a]

[a] Department of Civil and Environmental Engineering, University of Strathclyde, Glasgow, UK
[b] StreamSim Technologies Inc., San Francisco, CA, USA
[c] Department of Energy Resources Engineering, Stanford University, CA, USA

ARTICLE INFO

Keywords:
Carbon capture & storage
Microbially induced carbonate precipitation
Well sealing
Calcite dissolution
Multiphase flow
X-ray CT

ABSTRACT

Microbially induced carbonate precipitation (MICP) is a novel method for controlling permeability in the subsurface with potential for sealing or reducing leakage from subsurface engineering works such as carbon sequestration reservoirs. The purpose of this research was to measure, at core scale, the change in reservoir permeability and capillary pressure due to MICP during seal formation, then to monitor the integrity of the seal when exposed to acidic groundwater capable of causing dissolution. The experiment was carried out with a Berea sandstone core mounted in a high pressure core holder within a medical X-ray CT scanner.

Multiple full volume CT scans gave spatially resolved maps of the changing porosity and saturation states throughout the experiment. Porosity and permeability decreased with MICP whilst capillary pressure was increased. Dissolution restored much of the original porosity, but not permeability nor capillary pressure. This lead to the conclusion that injection pathways were coupled with carbonate precipitation hence preferential flow paths sealed first and transport of the dissolution fluid was limited. Provided a high enough reduction in permeability can be achieved over a substantial volume, MICP may prove to be a durable bio-grout, even in acidic environments such as a carbon sequestration reservoir.

1. Introduction

Microbially induced carbonate precipitation (MICP) is a process in which bacteria (e.g. the soil bacteria *Sporosarcina pasteurii*) mediate a biochemical reaction that can result in the precipitation of calcium carbonate. *S. pasteurii* produces the enzyme urease which hydrolyses urea, ultimately producing ammonium, carbonate and a pH increase (Ferris et al., 2003). When urea hydrolysis takes place in the presence of a calcium source such as calcium chloride ($CaCl_2$), the pH increase and the production of carbonate lead to $CaCO_3$ precipitation with the bacteria acting as nucleation points for crystal growth (Ferris et al., 2003). This MICP process has been investigated for several purposes including: improving strength and stiffness of porous media whilst maintaining permeability (DeJong et al., 2010; van Paassen, 2009; Whiffin et al., 2007); permeability reduction in porous media (Handley-Sidhu et al., 2013; Mitchell et al., 2013; Tobler et al., 2012); immobilising pollutants (Fujita et al., 2008; Mitchell and Ferris, 2005) and producing self-healing concrete (Jonkers et al., 2010). El Mountassir et al. (2014) previously assessed the suitability of MICP for fracture grouting under constantly flowing conditions and observed the formation of dendritic-like preferential flow paths due to hydrodynamic feedback.

MICP may be an ideal grout for reducing leakage from carbon sequestration reservoirs, specifically at the host rock/cement interface of cemented injection wells, and has been considered for this purpose by Cunningham et al. (2014), Phillips et al. (2016) and Verba et al. (2016). Unlike cement based grouts, the MICP injection fluids have a very low particle size (0.5–5 μm for individual bacterial cells (van Paassen, 2009), average 2.8 μm (Tobler et al., 2014)), and water-like viscosity enabling excellent penetration into narrow aperture fractures and porous media with low injection pressures: compared with a microfine cement (viscosity 50 mPa s), MICP fluids (viscosity 1.1 mPa s) would require an injection pressure 45.5 times lower, enabling injection at a higher volumetric flow rate or the use of lower pressure injection equipment. Unlike low viscosity chemical grouts with a design life of, at best, decades (Woodward, 2005), natural analogues suggest calcium carbonate sealed flow pathways may remain sealed over the 10,000 years in which injected CO_2 must reside in the formation for effective climate mitigation (Shaffer, 2010). MICP is also both less expensive (Gallagher et al., 2013; Ivanov and Chu, 2008; Suer et al., 2009) and less toxic than many chemical grouts.

* Corresponding author.
E-mail address: james.minto@strath.ac.uk (J.M. Minto).

http://dx.doi.org/10.1016/j.ijggc.2017.07.007
Received 22 September 2016; Received in revised form 14 April 2017; Accepted 10 July 2017

The CO_2 rich groundwater in a sequestration reservoir can be expected to be acidic (Sigfusson et al., 2015), potentially resulting in $CaCO_3$ dissolution (Dawson et al., 2015; Iglauer et al., 2014) and raising questions about the longevity of an MICP seal. Mitchell et al. (2013) investigated the dissolution of microbially precipitated $CaCO_3$ in batch reactors at both reservoir and atmospheric pressures and found rapid dissolution in a matter of hours, but note that in a porous media, reaction rates may be limited by transport of the acidic water to the $CaCO_3$ surface. Numerous flow-through $CaCO_3$ dissolution experiments in porous media have been carried out (Boever et al., 2012; Ellis et al., 2013; Luquot and Gouze, 2009; Menke et al., 2015), however in these experiments the $CaCO_3$ formed abiotically and therefore without the feedback between flow paths, bacterial attachment and $CaCO_3$ precipitation observed by El Mountassir et al. (2014) during MICP sealing of fractured rock.

The aim of this paper is to measure, at the core scale, changes in reservoir permeability and capillary pressure due to microbially induced precipitation of $CaCO_3$ and its subsequent dissolution, within a rock representative of a sequestration reservoir. Furthermore, by measuring spatial variations in the amount of precipitated $CaCO_3$, it is possible to assess the effectiveness of the seals formed by this process. This will allow evaluation of MICP's potential as a tool for reducing leakage from sequestration reservoirs, whilst also shedding light on the diagenesis of natural carbonate cemented sandstones.

2. Experimental methods

Experiments consisted of precipitating calcium carbonate within a sandstone core via MICP, then dissolving the $CaCO_3$ with the injection of low pH fluids, as summarized in Fig. 1. The sandstone core was mounted in a high pressure core holder. Permeability was measured several times over the course of the experiment. X-ray attenuation of the core was measured at intervals with X-ray computed tomography to obtain 3D maps of the change in porosity and degree of saturation throughout the core.

2.1. Sandstone core properties

The core used in these experiments was quarried from the Upper Devonian Berea sandstone formation in Ohio, USA. Berea from this quarry typically consists of predominantly sand-sized quartz grains cemented by silica with minor presence of iron oxide (93.13% SiO_2, 3.86% Al_2O_3, 0.54% FeO, 0.25% MgO, 0.11% Fe_2O_3, 0.10% CaO) (Cleveland Quarries, 2017). The core had no visible bedding planes, had been cut to 50.8 mm (two inch) in diameter and 100 mm long, and had been fired at 700 °C to stabilize any swelling clays. This core had previously been extensively characterized and used in multiphase flow experiments by Krevor et al. (2012) who described the core as typical of Berea sandstones, well sorted with submature granular features and found minimal porosity variation along the core length.

2.2. MICP injection fluid preparation

Three components are required for MICP: an ureolytically active bacterial strain (*Sporosarcina pasteurii*), a calcium source (calcium chloride), and urea which, when hydrolysed by the urease enzyme, provides the carbonate component of the calcium carbonate and increases the pH facilitating the precipitation of the calcium carbonate.

To prepare bacterial suspensions, *S. pasteurii* was initially grown on Brain Heart Infusion (BHI) agar (37 g/l) with syringe filter sterilised urea (20 g/L). A single colony was then transferred using aseptic technique to BHI broth, again containing syringe filtered urea (20 g/L), and grown overnight at ~30 °C in a shaker incubator. The bacteria were separated from the growth medium by centrifugation (at 6000 rpm for 8 mins) and re-suspended with tap water (sterilised by autoclaving) to the desired optical density (OD_{600}, i.e. measured at a wavelength of 600 nm using a UV–vis spectrophotometer). Fresh bacterial suspensions were prepared daily and approximately 100 ml BHI broth yielded 100 ml of centrifuged and re-suspended bacterial suspension.

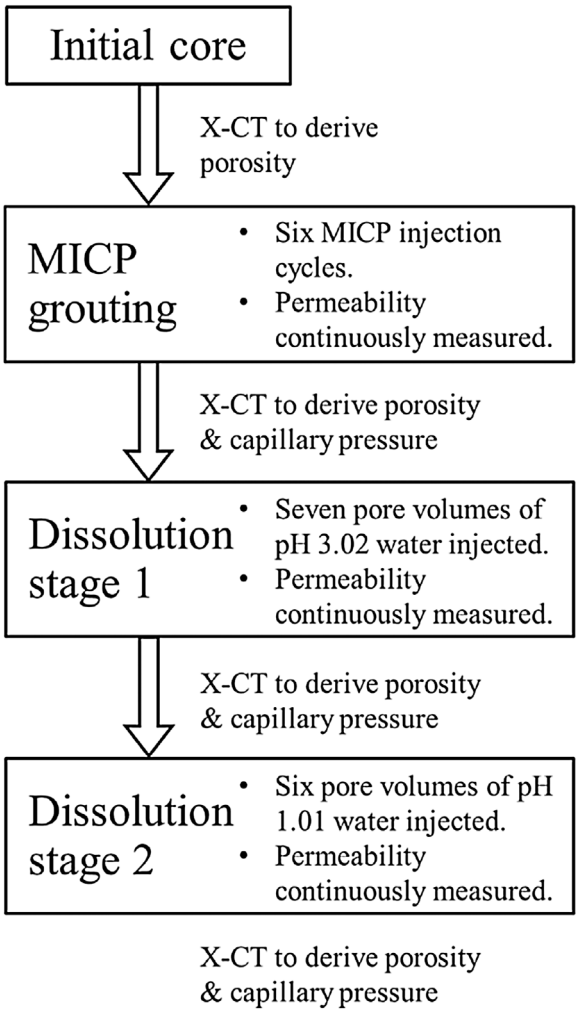

Fig. 1. Summary of experimental itinerary.

The urea-$CaCl_2$ solution is comprised of 0.2 M $CaCl_2$ (22.20 g/l) and 0.4 M urea (24.02 g/l) and is adjusted to a pH of 6.5 using HCl. Dissolution fluid consisted of DI water pH adjusted to 3.02 (stage 1) and 1.01 (stage 2) with HCl. Details of the number of injections and their volumes are presented in Table 1.

2.3. MICP injection strategy

Several fluid injection strategies exist for the many different applications MICP has been suggested for:

- Simultaneously injecting *S. pasteurii* and urea-$CaCl_2$ solution, then, once the pore space is saturated, ceasing injection so that precipitation occurs under static conditions.
- Stimulating the growth of an *S. pasteurii* biofilm inside the porous media, then saturating the media with injected urea-$CaCl_2$ solution, followed by a static (no injection) period over which precipitation occurs.
- Injecting bacteria, allowing a static period for bacterial attachment to the surface of the porous media (sometimes aided by the addition of a "fixer", e.g. 0.05 M $CaCl_2$, that encourages flocculation), then injecting urea-$CaCl_2$ solution followed by a cessation of flow and $CaCO_3$ precipitation under static conditions. Multiple cycles of

Table 1
MICP fluid injection strategy. Between each bacterial and urea-$CaCl_2$ injection was a 15 ml tap water pulse to prevent precipitation within the tubing. Overnight between cycles 3 and 4, and after cycle 6, the core was flushed with ten pore volumes of tap water allowing flow to be turned off overnight without precipitating $CaCO_3$ under non-flowing conditions.

Day	Cycle	Bacterial suspension			urea-$CaCl_2$ solution			
		OD_{600} [−]	Volume [mL]	Q [mL/min]	CaCl2 [M]	Urea [M]	Volume [mL]	Q [mL/min]
1	1	0.90	100	5	0.2	0.4	300	5
	2	0.90	100	5	0.2	0.4	300	5
	3	0.91	100	5	0.2	0.4	300	5
2	4	0.71	100	5	0.2	0.4	300	5
	5	0.73	100	5	0.2	0.4	300	5
	6	0.81	100	5	0.2	0.4	300	5

bacteria then urea-$CaCl_2$ solution are required and $CaCO_3$ is progressively precipitated with each cycle.

These three methods require delivery of both bacteria and urea-$CaCl_2$ solution into the pore space where the reaction occurs and rely on periods of no flow during which the majority of the precipitation occurs. In many applications, these static conditions will not exist due to the continuous movement of groundwater. El Mountassir et al. (2014) found that, under continuously flowing conditions, feedback between hydrodynamics and precipitation occurred leading to the formation of stable open channels, whilst Minto et al. (2016) found that more uniform precipitation could be achieved in rock fractures through the use of lower injection rates and flow velocities. In this study, to investigate the important issue of the potential for channel formation during MICP, we employ a fourth injection strategy: sequential injection of bacteria followed by urea-$CaCl_2$ solution with no static period for bacteria attachment or calcite precipitation.

Studies of MICP in sandstone are limited, and to our knowledge, there are no MICP experiments under continuously flowing conditions in sandstone. Tobler et al. (2014) studied the transport of *S. pasteurii* through Bentheimer sandstone cores with bacterial optical densities of 0.1, 0.5 and 1.0, flow rates of 1 or 3 ml/min, and core lengths between 1.8 and 7.5 cm. Sham et al., 2013 used magnetic resonance imaging to detect spatial variation in microbially induced $CaCO_3$ formation inside a Bentheimer sandstone core with a bacterial OD_{600} of 0.45 injected for two hours, followed with a two hour static period for attachment, then one hour of 1 M $CaCl_2$/1 M urea solution with a one day static period for precipitation. 22 injection cycles (hence 22 days) were required to reduce permeability from 1023.4 mD (1.01 μm^2) to 35.5 mD (0.035 μm^2).

For a core-scale analogue to reservoir sealing and well leakage reduction, we desired a significant reduction in permeability, but with more rapid precipitation than Sham et al. (2013), and continuous flowing conditions to counter groundwater movement. Minto et al. (2016) found that greater amounts of bacteria led to a greater final mass of $CaCO_3$ precipitated and that, in a flowing system, the greatest reduction in permeability occurred in the first three hours of each urea-$CaCl_2$ cycle, as afterwards the bacteria became encased in $CaCO_3$ thus limiting their access to urea.

To this end, a high bacteria concentration (between 0.71–0.91 OD_{600}) was chosen and short urea-$CaCl_2$ injections were used. MICP at reservoir temperature and pressure has been shown to be possible with *S. pasteurii* by Mitchell et al. (2013) and Verba et al. (2016). Maintaining reservoir pressures in the core holder setup (shown in Fig. 2) whilst the MICP fluids were injected in cycles would not allow injection at a constant flow rate. As the potential for hydrodynamic feedback between flow, $CaCO_3$ precipitation, and resultant preferential flow path formation were the main focus of this paper, the core outlet was kept at atmospheric pressure during all MICP injections to enable constant flow rate injections. Temperature was 20 °C. In total there were six injection cycles over a two-day period (Table 1) with continuous injection of either bacteria or urea-$CaCl_2$ at a volumetric flow rate of 5 ml/min. At the end of day 1, cycle 3, and again at the end of day 2, cycle 6, the core was flushed with ten pore volumes of non-sterile tap water delivered at 5 ml/min to prevent any precipitation while pumps were turned off. Between each injection of bacteria and urea-$CaCl_2$ was a 15 ml injection of tap water to clean and prevent $CaCO_3$ precipitation in the tubing.

2.4. Dissolution stages

Dissolution took place in two stages as it was critical to capture dissolution mid-way through the process i.e. when a change in permeability and porosity was measureable, but when dissolution had not progressed to a point where all the microbially precipitated carbonate had been stripped. The first stage of dissolution informed when that point might be reached whilst the second stage accelerated dissolution to achieve it within a reasonable experimental timeframe.

Dissolution consisted of injecting deionized water, in which the pH had been adjusted with hydrochloric acid, as a surrogate for low pH, CO_2 saturated groundwater. The initial stage consisted of seven pore volumes of pH 3.02 to test the response of the system under realistic conditions (pH 3.02 is representative of CO_2 saturated brine at reservoir conditions). The second more aggressive dissolution stage consisted of six pore volumes of pH 1.01. Effluent pH was continuously monitored, as was pressure drop across the core. After each dissolution stage, the core was flushed with ten pore volumes of non-sterile tap water to ensure that no dissolution fluid remained within the core.

All dissolution fluids were injected at 5 ml/min and with the core outlet at atmospheric pressure. This was necessary to prevent $CaCO_3$ saturated water recirculating within the injection and backpressure pumps, the phase separator, and the connecting lines as the eventual decrease in pressure at the end of a high pressure experiment would cause the fluid to become super-saturated with respect to $CaCO_3$ and precipitation throughout the equipment.

2.5. Multiphase & MICP injection equipment

The experimental setup was adapted from that used by Perrin and Benson (2010), Krevor et al. (2012) and Pini et al. (2012) for multiphase core flooding experiments, to include a fluid volume exchange device (VED) fitted between the liquid injection pump and the core. This setup, shown in Fig. 1, allows 1) utilising the VED for low pressure (2 MPa max) injection of bacteria and urea-$CaCl_2$ solution, or dissolution fluid, with the core outlet open to atmosphere for sample collection, and 2) bypassing the VED for injection at reservoir temperature and pressures (in this case 50 °C and 8.96 MPa) to characterise core flow properties in a re-circulating system.

Injection of water into the rock core for permeability measurement and N_2 for capillary pressure measurement was controlled by two dual syringe pumps (Teledyne Isco 500D, max pressure 25.9 MPa). Temperature was controlled via water bath heat exchangers that preheated the injection fluids, and with electric heating bands that maintained this temperature within the core. A phase separator (TEMCO AMS-900, max pressure 68.9 MPa) collected the core effluent,

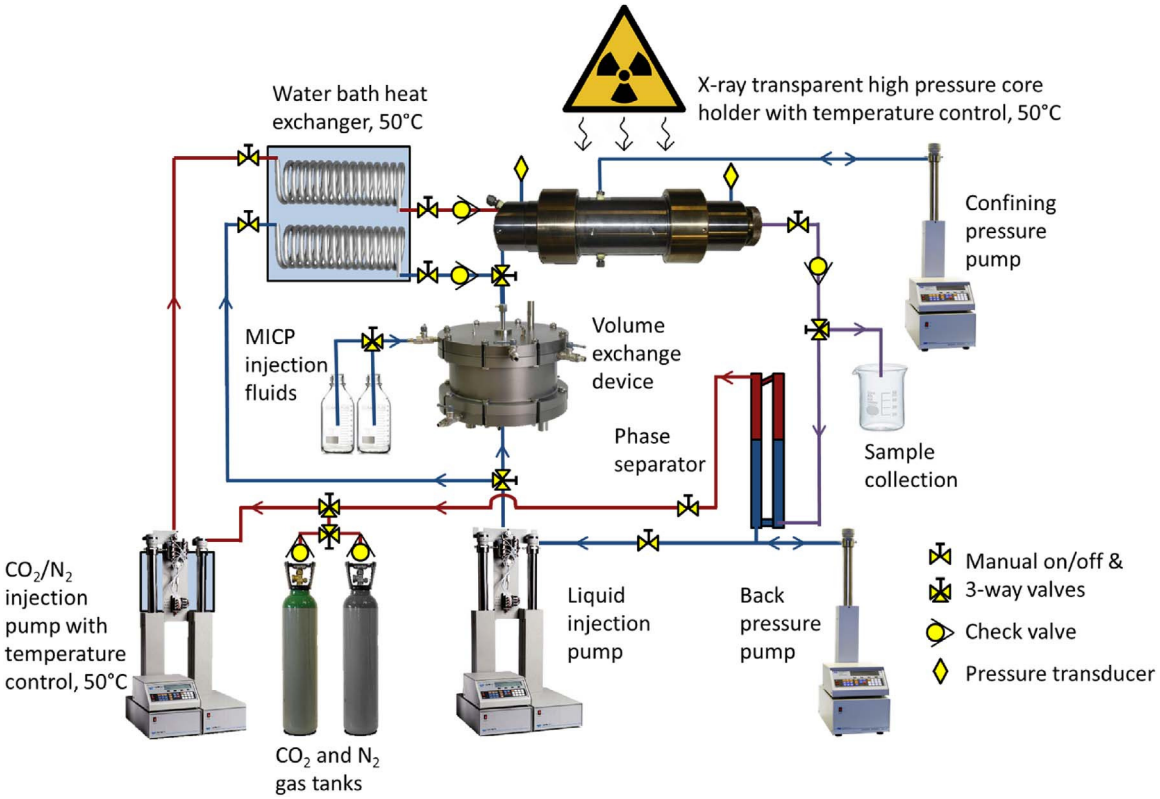

Fig. 2. Multiphase core-flooding setup allowing continuous re-circulating injection of fluids at reservoir temperatures and pressures. MICP fluids (bacteria, urea, $CaCl_2$) injected at low pressure (2 MPa max) via the volume exchange device connected between the liquid injection pump and the core holder.

separated the phases and diverted them to the appropriate pumps allowing continuously recirculating fluid injection. Back pressure was maintained on the core through the water phase with a syringe pump (Teledyne Isco 1000D, max pressure 13.8 MPa) connected 'downstream' of the phase separator. Confining/overburden pressure was applied to the core via an additional syringe pump (Teledyne Isco 260D, max pressure 51.7 MPa). Pressure drop across the core was measured with two high accuracy pressure transducers (Oil filled Digiquartz Intelligent Transmitter, model 9000-3K-101, accuracy typically better than 2 KPa) connected immediately upstream and downstream of the core.

The VED was necessary to prevent any mixing of bacteria and urea-$CaCl_2$ solution, and hence $CaCO_3$ precipitation, within the pumps. Three way valves were used to connect the VED to the liquid pump and to the core allowing the VED to be bypassed during injections under reservoir conditions, and for the liquid pump to be used to both refill and inject the MICP fluids without these fluids entering the pump. MICP fluid injection volumes were limited to 100 ml (the volume of the VED), to a pressure of 2 MPa, and the VED was rinsed with non-sterile tap water between bacteria and urea-$CaCl_2$ solution cycles to prevent $CaCO_3$ precipitation within the VED and tubing.

2.6. X-ray scan acquisition and analysis

The X-ray system used was a General Electric Hi-Speed CT/i: a medical scanner that allows imaging of dense samples (such as a 50.8 mm diameter sandstone core inside a high pressure core holder) with a resolution of 0.5 × 0.5 × 1 mm (x,y,z) over a reconstructed field of view of 25 cm. Tube current was 200 mA and electron energy was 120 keV. Full volume scans consisted of 104 slices (each 1 mm thick) from inlet to outlet and took 19 min to acquire. Additional scans of the inlet section were made to reduce error in measurement of the inlet slice saturation: averaging multiple scans has been shown by Pini et al. (2012) to improve signal to noise ratio. A full list of scans can be found in Table S1, Supplementary information.

Single scans gave average X-ray attenuation and hence average density of each voxel. Multiple full volume and inlet section scans were made to determine average attenuation during fully saturated, fully unsaturated, and partially saturated conditions. A combination of the fully saturated and fully unsaturated attenuations with reference attenuations for water and N_2 at 8.96 MPa gave the average porosity of each voxel (Eq. (1)). A combination of the partially saturated attenuation with that of the fully saturated and fully unsaturated gives the voxel averaged degree of saturation (Eq. (2)). CT_w and CT_a refer to the reference attenuation of the wetting (water) and non-wetting (N_2) phases respectively. $CT_{wr,i}$ and $CT_{ar,i}$ refer to the attenuation of the fully wetting phase saturated and fully non-wetting phase saturated rock core for every voxel, i, of the entire scanned volume. $CT_{awr,i}$ refers to the partially saturated conditions arising when N_2 was injected into the water saturated core during the capillary pressure measurement.

$$porosity = \frac{CT_{wr,i} - CT_{ar,i}}{CT_w - CT_a} \quad (1)$$

$$S_{N\,2} = \frac{CT_{wr,i} - CT_{awr,i}}{CT_{wr,i} - CT_{ar,i}} \quad (2)$$

Raw X-ray CT data was reconstructed with the scanner's built in software. Analysis of the reconstructed data and the calculation of porosity and N_2 saturation was made with FIJI distribution of image analysis software ImageJ (Schindelin et al., 2015). Paraview (Ahrens et al., 2005) was used for data visualization in 3D.

Pressure at the core inlet and outlet was measured continuously at ten second intervals to get pressure drop across the core. Combined with the known flow rate supplied by the water pump, permeability was measured at each stage of the $CaCO_3$ precipitation and dissolution process. Each permeability measurement was made at three different flow rates under fully water saturated conditions.

Fully water saturated conditions were achieved by flushing injection

lines and the core with CO_2 at atmospheric pressure to displace all air within the system. Water was then flushed through the core at a low flow rate and at atmospheric pressure for several pore volumes then core pressure was increased to 8.96 MPa. Ten pore volumes of water were then flushed through the core at 8.96 MPa over which time it was assumed that all residual CO_2 would have dissolved into the water. Continuous monitoring of pressure drop across the core during this procedure indicated that pressure drop did reach a stable minimum value and hence residual CO_2 had been removed from the core leaving the core fully water saturated.

After $CaCO_3$ precipitation and again, after the second stage of dissolution, capillary pressure was measured by injecting N_2 into the water saturated core until steady state saturation conditions were reached (ensured by injecting ten pore volumes of N_2), measuring the degree of saturation with a full volume scan and multiple scans of the inlet, then increasing the N_2 injection flow rate and repeating. The degree of saturation in the inlet slice (using the average of the multiple scans to increase signal to noise ratio and hence accuracy) together with the pressure drop across the core can be used to calculate a capillary pressure curve, as described by Pini et al. (2012). In a previous experiment using the same core, Krevor et al. (2012) measured capillary pressure by mercury intrusion on a representative subsection of the unaltered rock. The change in capillary pressure due to $CaCO_3$ precipitation and its subsequent dissolution can be used to understand how the multiphase fluid transport properties of the core were altered.

In order to characterise the spatial heterogeneity of porosity observed within the core we calculated experimental variograms for each slice. The variogram, $\gamma(h)$, of the porosity $\phi(x)$ can be defined as:

$$\gamma(h) = \frac{1}{2} var(\phi(x+h) - \phi(x)) \tag{3}$$

where *var* is the statistical variance and h is distance (de Marsily, 1986). In practice, $\gamma(h)$ is the variance of the difference between all pairs of measured data points that are a lag distance, h, apart.

Fig. 3 illustrates the concept of a semi-variogram, which is to provide a measure of the degree of spatial correlation within a random field. Where there is no spatial correlation (i.e. Gaussian noise, Fig. 3) the variogram has an approximately constant value, equal to the background variance of the field (X-ray attenuation in our case). Where a field is spatially correlated, for pairs of measurement points that are close together (i.e. h is small) the variogram is close to zero, since the pairs of points are likely to have similar values. As the distance between pairs increases, the variogram asymptotically tends to the background variance of the field. The higher the degree of spatial correlation in the field, the greater the lag distance along the x-axis before the variogram reaches the background variance.

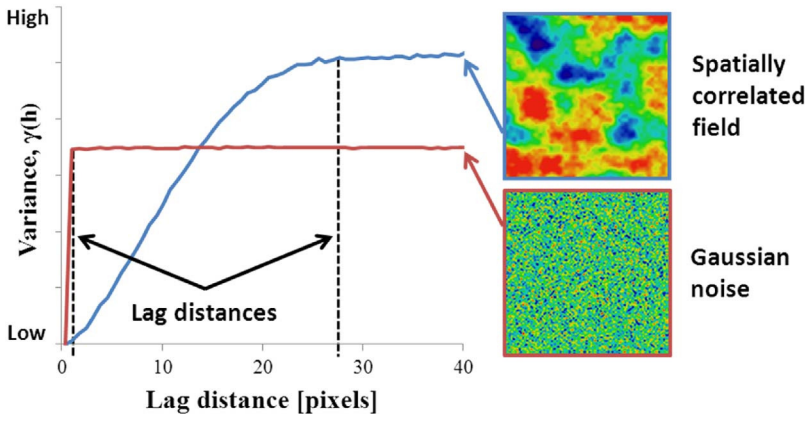

Fig. 3. Example semi-variograms for spatially correlated and uncorrelated fields.

2.7. Core inlet region

Due to the 1 mm X-CT slice thickness, each voxel of the core inlet and outlet slice will contain partly Berea core and partly the aluminum distribution platen of the core holder, with the proportion of each dependent on exactly how the core holder was positioned in the scanner. For core flooding experiments, these first and last slices are typically discarded and only those slices that contain 100% core are used for further analysis (e.g. Perrin and Benson, 2010; Krevor et al., 2012; Pini et al., 2012). For MICP, particularly when injecting into cores with relatively small pore throats, it is possible both for bacteria to be physically strained in the media causing permeability reduction due to biomass clogging (Mitchell et al., 2009) and for $CaCO_3$ to precipitate on the inlet face rather than in the core.

To enable characterisation of the core inlet, the core was subsequently scanned using a Nikon XT H 320 X-ray micro CT scanner. This scan had to be conducted after completion of the MICP and dissolution stages, as core flooding experiments inside the micro CT system were not possible. Details of the micro CT scan acquisition settings and image processing can be found in the Supplementary information. Using the X-ray micro CT scan data, porosity could be measured by segmenting the image into solid and pore space (rather than from the combination of air saturated and water saturated scans). Analysis was restricted to the first 2 mm of the core: the first millimetre to capture the inlet face and region that could not be captured with the medical CT; the second millimetre to establish continuity between the porosity measurements utilising the two different X-ray systems and techniques.

3. Results

A $CaCO_3$ seal was successfully precipitated within the core and then partially dissolved. Results are interpreted with respect to: change in permeability and capillary pressure at the core scale; average values of porosity and variation in X-ray attenuation from inlet to outlet; and fully 3D representations of porosity (Fig. 3) at each stage of $CaCO_3$ precipitation and dissolution.

The 3D data sets consist of slices acquired with fan-beam X-ray CT. Each slice was acquired independently with the sample table motor moving the core through the fan-beam in 1 mm increments. This resulted in 104 slices from core inlet to outlet (100 of the core, two of both the inlet and outlet for positioning) with a longitudinal resolution of 1 mm. Transverse resolution of each slice was 0.5 × 0.5 mm.

3.1. Core average $CaCO_3$ precipitation and dissolution

Monitoring core effluent during all MICP injection cycles showed that OD_{600} was constant and that no measureable amount of bacteria escaped the sandstone. Effluent pH during dissolution reached a

Table 2
Change in permeability throughout experiment.

Scan	Permeability [mD]	% of original permeability
Pre-MICP	885.74	100
Post-MICP	39.60	4.47
Dissolution stage 1	66.19	7.47
Dissolution stage 2	47.56	5.37

minimum of 7.04 during the first (pH 3.02 injected) dissolution stage and 3.83 during the second (pH 1.01 injected).

Table 2 outlines core averaged permeability change over the duration of the experiment. The six MICP cycles resulted in a 95.53% reduction in permeability (886–39.6 mD). Permeability reduction occurred during the urea-$CaCl_2$ injection, not the bacterial injection of each MICP cycle, with the exception of the final injection (cycle 6) in which permeability dropped during both bacterial injection and urea-$CaCl_2$ injection.

The first stage of dissolution restores some permeability (up to 66.2 mD), yet, somewhat unexpectedly, the second stage of dissolution reduces permeability to 47.6 mD. This reduction in permeability was attributed to migration of fines or re-precipitation of $CaCO_3$ (see Section 4.3).

3.2. Spatial heterogeneity in $CaCO_3$ precipitation and dissolution

To understand how the bulk permeability change in Table 2 is related to the pattern of precipitation and dissolution throughout the core, we consider average values within each slice, with each slice taken in the axial direction (perpendicular to the direction of flow).

Slice averaged porosities, calculated from fully water saturated and fully N_2 saturated scans with equation 1, are shown in Fig. 5. Initial (pre-MICP) slice averaged porosity was 20.6% and highly uniform from inlet to outlet. $CaCO_3$ precipitation resulted in a discernible decrease in porosity up to 51 mm into the 100 mm core. The maximum decrease in porosity within this region was 4.3% (at the inlet slice) with an average decrease in porosity of 1.2% over the first 51 mm.

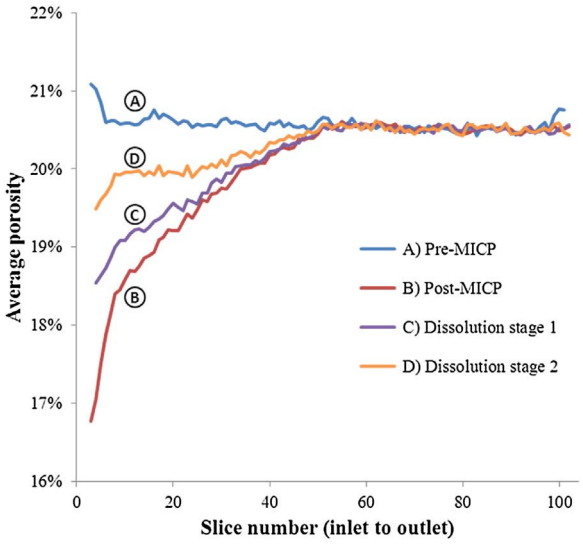

Fig. 5. Slice averaged porosity before and after initial $CaCO_3$ precipitation followed by two subsequent stages of dissolution. Inlet slices (1,2) and outlet slices (103,104) removed as these are affected by the core holder end caps. Precipitation limited to the first 51 slices and hence the first 51 mm of the core.

Dissolution stages 1 and 2 each restored some porosity: 0.3% (average) by stage 1 and 0.7% (average) by stage 1 and 2 combined. There was no discernible change in the porosity of the core beyond 51 mm during precipitation. Dissolution stage 1 dissolved $CaCO_3$ up to 33 mm into the core whilst stage 2 increased dissolution up to 46 mm (Fig. 5).

3D trends in $CaCO_3$ are clearly visible in the visualization of the X-ray CT data, both after precipitation and after each subsequent stage of dissolution (Fig. 4). To quantify these trends within slices perpendicular to the flow direction, porosity histograms for each slice were plotted (Fig. 6), revealing the initial porosity to be normally distributed within each slice and highly uniform between slices. Post-MICP precipitation, the slices retain a normal distribution, but with a shift towards lower

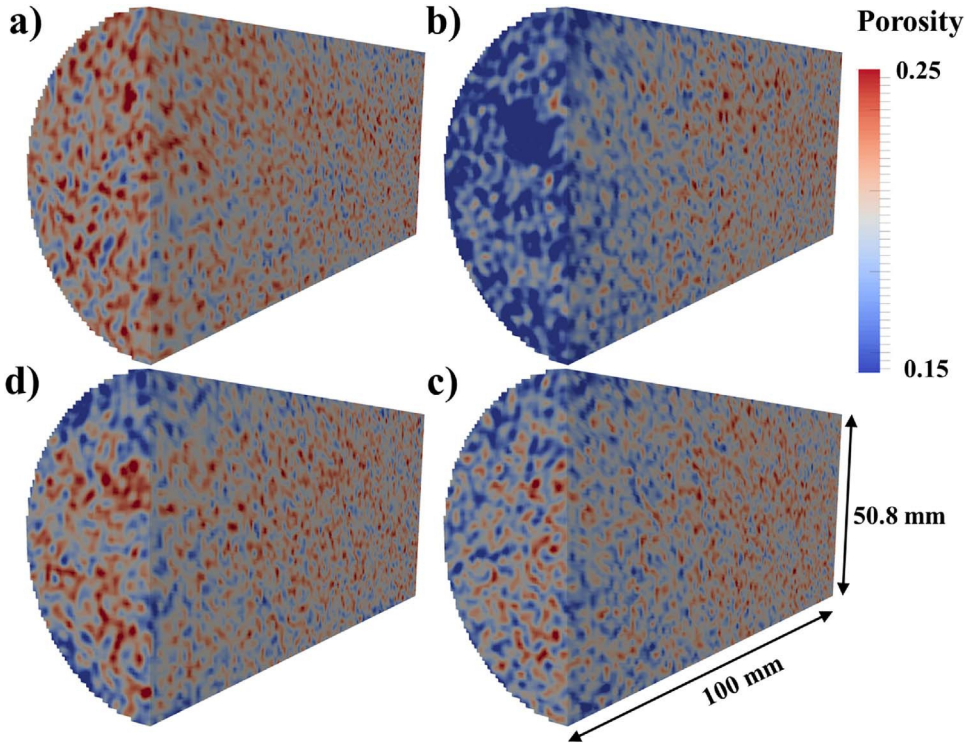

Fig. 4. 3D visualization of porosity in half-sections of the core a) pre-MICP precipitation, b) post-MICP precipitation, c) dissolution stage 1, and d) dissolution stage 2. The majority of $CaCO_3$ precipitation occurs at the inlet, extending up to 51 mm into the core.

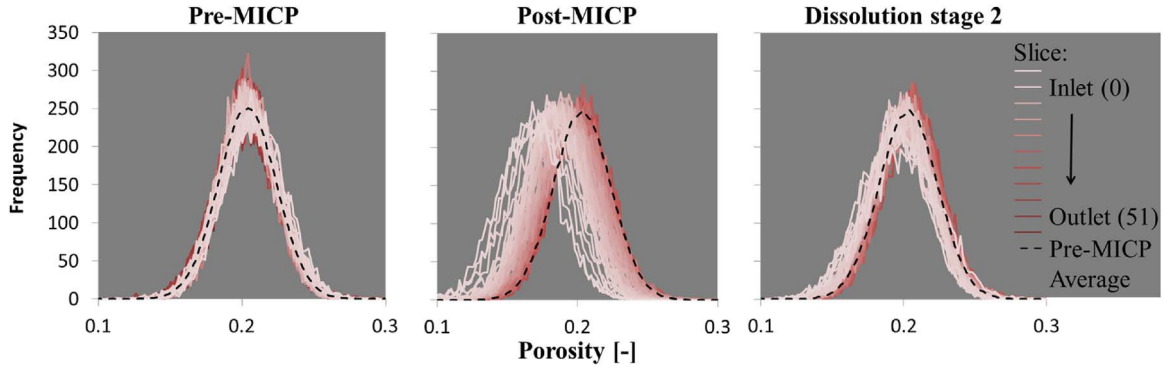

Fig. 6. Histograms of porosity variation within each slice shown for the volume in which $CaCO_3$ was precipitated (slices 0–51) for the pre-MICP, post-MICP and after dissolution stage 2. For reference, the average histogram of the pre-MICP core is superimposed upon each.

porosities and a slight widening in the porosity range, the magnitude of which was greatest close to the inlet. After the second stage of dissolution the porosity histograms were partially restored to their initial values.

3.3. Multiphase property characterisation

Initial capillary pressure measurements were made by mercury intrusion on a representative sample of the Berea sandstone, as detailed in Krevor et al. (2012), and converted to a water/N_2 system taking interfacial tension to be 65 mN/m for N_2 and 485 mN/m for mercury and assuming contact angles for the two systems were equal. $CaCO_3$ precipitation resulted in a substantial increase in the capillary pressure required to achieve a given N_2 saturation. Dissolution resulted in only a small return towards the initial pre-MICP capillary pressure, matching the pattern of change observed for core scale permeability.

A Brooks-Corey model was used for capillary pressure with gas entry pressure (P_e) and pore size distribution index (λ) used as fitting parameters (Table 3). Sw_{irr}, the irreducible water saturation, had previously been approximated for the pre-MICP condition as the difference between porosity measured by mercury intrusion and by the X-ray CT method calculated with Eq. (1). The model was fitted for the MICP and dissolution altered cores, with the assumption that Sw_{irr} remained constant (Fig. 7).

3.4. CT number semi-variograms

Sub-millimetre alignment errors between each scan may have arisen due to the limited accuracy of the CT scanner table movement in to, and out of, the scanner as table movement was limited to 0.5 mm increments. By considering the CT number of each individual dataset instead of porosity and saturation (the derivation of which both require a combination of multiple scans and hence multiple movements of the sample into and out of the scanner), the effect of any misalignment is eliminated. Hence, spatial correlation in the CT number was analysed as being representative of changes in the sandstone porosity structure due to precipitation and dissolution.

The semi-variograms (Fig. 8) reveal that pre-MICP precipitation, the variogram of the CT number is relatively constant, i.e. there is a random pore structure with almost no spatial correlation, which is consistent with the CT image of the inlet slice in Fig. 8a. Lag distance and the background variance were little changed by $CaCO_3$ precipitation, except for the first four slices adjacent to the inlet, showing that $CaCO_3$ precipitation was relatively uniform, after the first four slices. Visual observation of the CT number from the inlet slice after precipitation (Fig. 8a) clearly shows it to be more spatially correlated, with patches of low porosity. Dissolution further increased the lag distance and the background variance in the first 38 mm of the core, but again, only significantly so in the first four slices. This may indicate the formation of preferential flow paths within the first 4 mm of the 100 mm core; the CT scan at the inlet (Fig. 8a) shows large patches with high porosity.

3.5. Core inlet region

Upon removing the core from the core holder after MICP and dissolution, $CaCO_3$ precipitate was visible on the inlet face (Fig. 9a). Micro CT analysis (Fig. 9c–e) of a 13.5 mm diameter sub-sample revealed that from 1 mm to 2 mm into the core, porosity derived from segmenting the micro CT data with a global threshold, was comparable to that obtained from the combination of the air and water saturated scans from using the medical CT scanner (19.30% compared with 19.41%). The minimum slice average porosity was 16.26%, occurring 480 μm from the inlet face, and the majority of the pore space was connected, with only 0.34% disconnected pore space. N.B. the inlet face is considered here to be the first slice of the data in which any part of the Berea core is visible.

4. Discussion

4.1. Bacteria penetrability

Bacteria penetrability into the Berea core was low as no bacteria were detected in the effluent and was probably limited to the first 51 mm where $CaCO_3$ precipitation occurred. This is unsurprising given the bacterial cell size of 0.5–5 μm and the fine grained Berea, making physical straining of cells in pore throats likely as the main removal

Table 3
Brooks-Corey capillary pressure measurement fitting parameters. Pre-MICP capillary pressure measured with mercury intrusion by Krevor et al. (2012). * Sw_{irr} assumed to remain constant for the curve fitting.

Scan	Gas entry pressure P_e [Pa]	Irreducible water saturation, Sw_{irr} [−]	Pore size distribution index, λ [−]	Capillary pressure measurement range [Pa]
Pre-MICP (Krevor et al., 2012)	2.5×10^3	0.11	0.67	0–240 × 10^6
Post-MICP	6.734×10^3	0.11*	0.3079	8.09×10^3–68.86×10^3
Dissolution stage 2	4.363×10^3	0.11*	0.3075	8.62×10^3– 75.84×10^3

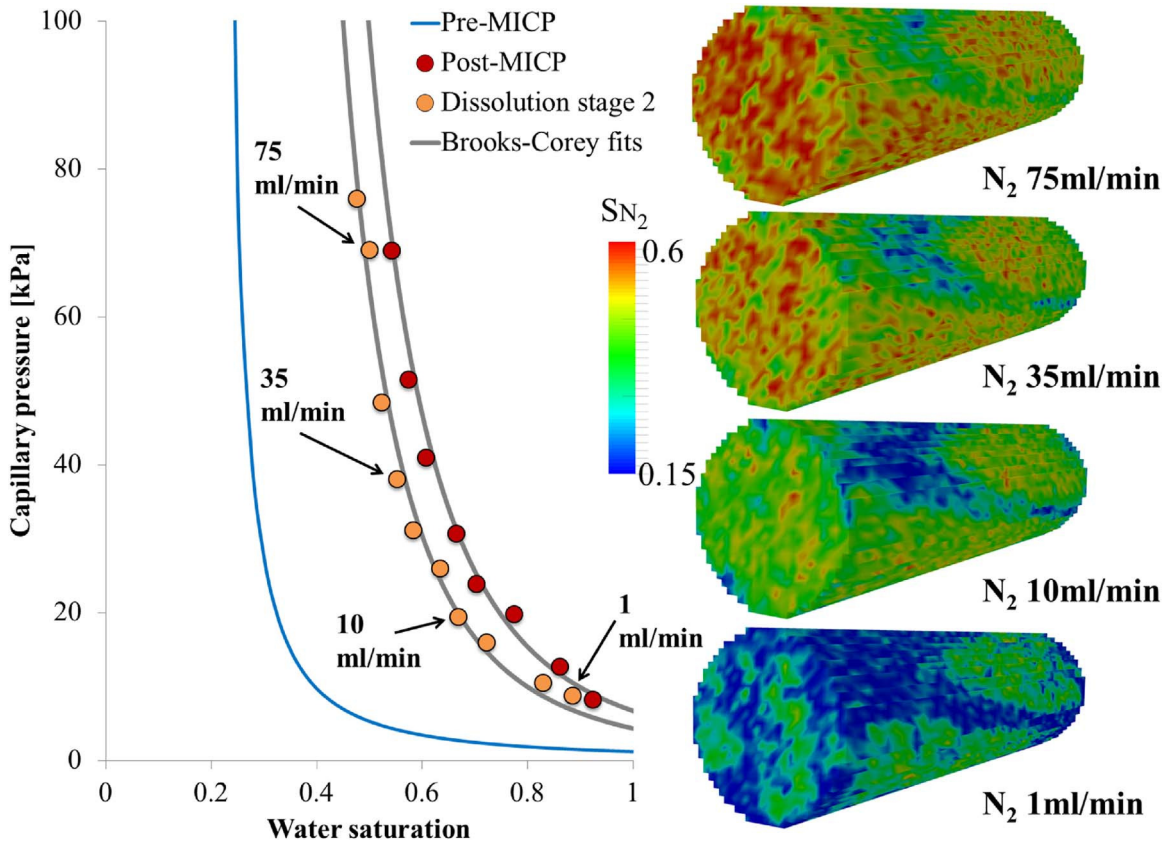

Fig. 7. Left: capillary pressure curves pre-MICP (from mercury intrusion (Krevor et al., 2012), adjusted to a H_2O/N_2 system), post-MICP, and post-dissolution stage 2. Right: measured N_2 saturation distributions at selected N_2 flow rates during the post-dissolution capillary pressure measurement.

mechanism. As bacterial transport through porous media is strain specific (Becker et al., 2003; Dong et al., 2002; Tufenkji, 2007), the study of *S. pasteurii* transport through Bentheimer sandstone by Tobler et al. (2014) is most relevant to this experiment. They recorded 24% bacteria recovery in the effluent of a 75 mm Bentheimer sandstone core when injecting a 1 OD_{600} *S. pasteurii* suspension at 3 ml/min and noted that percentage recovery decreased with increasing OD_{600} and with decreasing flow rate. The Bentheimer sandstone had a porosity of 23% and permeability of 2431 mD. Our 100 mm Berea core was longer and had a lower porosity and permeability which may explain why we saw zero bacteria recovery despite our lower injection OD_{600} (~0.8) and higher flow rate (5 ml/min).

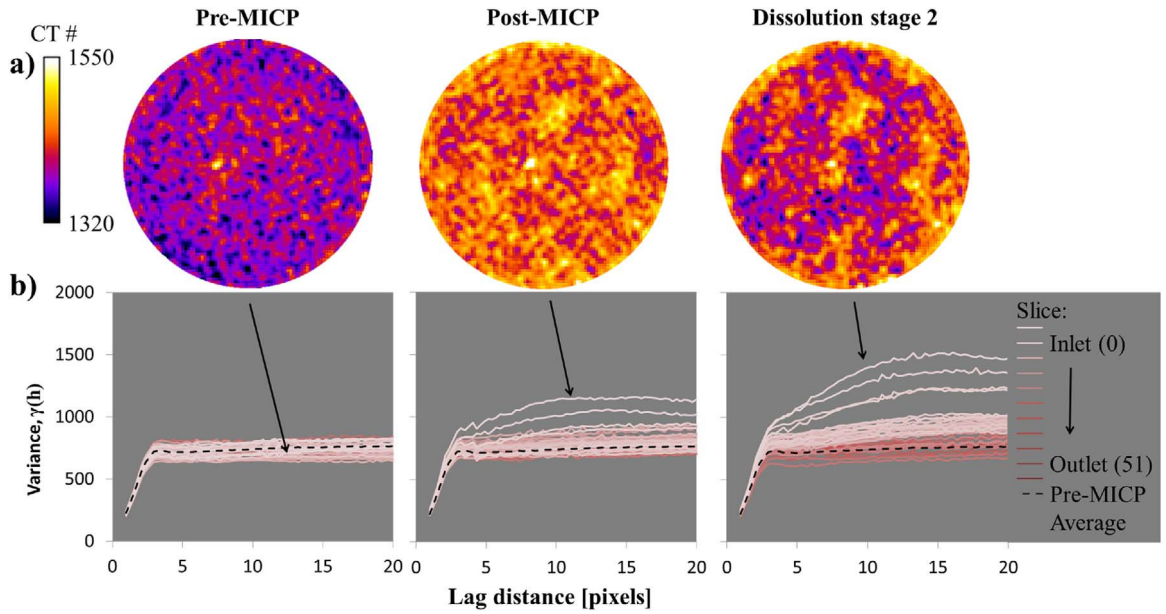

Fig. 8. a) Inlet slice CT numbers plotted for reference. Low CT numbers correspond to regions of high porosity. b) semi-variograms of CT number during a dry (N_2 saturated) scan for each slice along the core from the inlet (slice 0) towards the limit of $CaCO_3$ precipitation (slice 51).

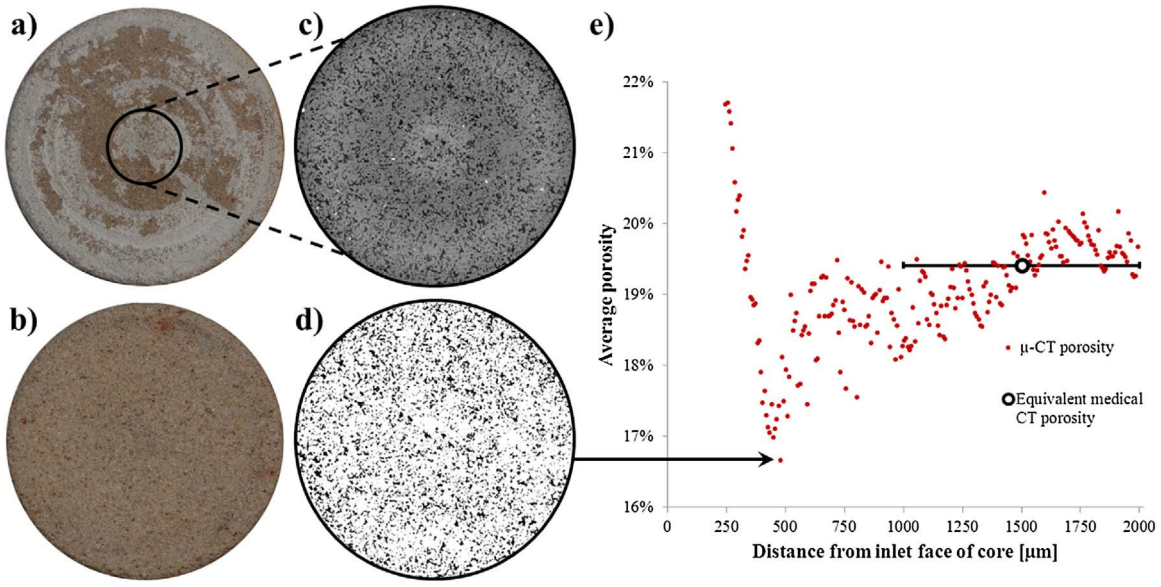

Fig. 9. Analysis of core inlet region after MICP and dissolution: a) core inlet face with white $CaCO_3$ precipitate, b) outlet face representative of unmodified core, c) X-ray micro CT of central sub-sample (slice with lowest porosity shown), d) binary segmentation of the same slice, and e) slice average porosity from inlet face to 2 mm into the core derived from the segmented micro CT data (with equivalent porosity from air and water saturated scans made with the medical CT scanner over a 1 mm section of core shown for reference).

4.2. Porosity and permeability reduction

The reduction in porosity brought about by the $CaCO_3$ precipitation was small, on average 1.2% in the first 51 mm of the core, yet there was a very large reduction in permeability (95.5% reduction). From the micro CT analysis of the first 2 mm of the core after dissolution, it is clear that the inlet face of the core was not sealed and could not have been solely responsible for the majority of this permeability reduction. Given the small increase in permeability upon dissolution, it is also highly unlikely that the inlet face was sealed prior to the dissolution stages.

The post-MICP porosity/permeability relationship may result from straining of bacteria in the pore throats throughout the first 51 mm of the core in which the porosity reduction was observed: the bacteria subsequently act as nucleation points for $CaCO_3$ precipitation hence only a small amount of $CaCO_3$ is required to block a pore throat and substantially reduce permeability.

As $CaCO_3$ precipitation occurs most rapidly where there is a high concentration of bacteria and adequate supply of urea-$CaCl_2$ solution, preferential flow paths are expected to fill with $CaCO_3$ first and for flow in subsequent injection cycles to be diverted along different paths, as has been observed in fracture sealing by MICP (Minto et al., 2016). A similar process of sealing in the highest permeability region followed by a shift to the next most permeable regions has been observed in sand packed columns (Harbottle et al., 2016; Mugwar, 2015). As a result, with each injection cycle the MICP fluids must take a progressively more difficult path through the core, requiring higher injection pressure.

4.3. Dissolution

Dissolution restored much of the porosity of the first 51 mm of the core, but very little of the permeability. This may be due to the pattern of precipitation noted earlier in which preferential flow paths are sealed first. The acidic water flows through the remaining 'less initially preferential' flow paths, where it becomes buffered by the dissolving $CaCO_3$. This results in an inability to dissolve the original preferential flow paths, meaning that permeability cannot return to its original value.

Permeability after the second stage of dissolution was actually lower than after the first stage of dissolution. Initially it was suspected that the more acidic water in the second stage led to such rapid dissolution that CO_2 gas bubbles were forming and becoming trapped, disconnecting some pore space and reducing that available for fluid flow thus appearing to reduce permeability. Completely drying and re-saturating the core proved this was not the case. Instead, it is more likely that dissolution dislodged fine particles near the inlet which then migrated through the porous media before lodging in pore throats and blocking them. Such a phenomenon has previously been observed in core-flood experiments by Ellis et al. (2013) and Mangane et al. (2013) involving the dissolution of carbonate rocks.

An alternative explanation is that $CaCO_3$ near the inlet was dissolving and saturating the fluid then, as this fluid was transported through the remaining preferential flow paths towards the outlet of the core, the $CaCO_3$ re-precipitated thus blocking the preferential pathway and diverting the flow elsewhere. Possible mechanisms for re-precipitation are the occurrence of supersaturated fluid due to mixing with higher pH water trapped in stagnant pore zones, a decrease in $CaCO_3$ solubility due to the change in pressure as fluid is transported from inlet to outlet, or simply abiotic crystal growth.

It is difficult to convert the results from this very low pH core dissolution experiment to a timeframe equivalent for conditions in a sequestration reservoir. Firstly, PHREEQC modeling (Parkhurst and Appelo, 2013) indicates approximately 60 times more $CaCO_3$ can be dissolved by the pH 1.01 fluid injected in this experiment than by reservoir brine at pH 3.02 (the expected pH of a generic sequestration reservoir) before reaching saturation (which is highly dependent upon major ion concentrations in the reservoir). Secondly, the pressure gradient across the 100 mm core was from 634 to 689 kPa/m during dissolution injection compared with, for example, the 9.41 kPa/m pressure gradient expected across the Goldeneye reservoir after reaching its maximum pressure (Shell U.K. Limited, 2014). What is clear is that the core was subjected to a dissolution rate, saturation capacity and flux of acidic fluid all far greater than would be encountered in a sequestration reservoir and dissolution can be expected to have been greatly accelerated. Nevertheless, these results show that even after a significant fraction of the porosity is restored from $CaCO_3$ dissolution, the permeability remains low.

4.4. Implications for sealing with MICP

Whilst this study was limited to a single core of a single rock type, when considering the processes taking place, the results are encouraging for the use of MICP for permeability reduction in mildly acidic conditions (such as a sequestration reservoir). The results show that, if a large reduction in permeability can be achieved, preferential flow paths will not exist, the flux of dissolution fluids through the barrier will be limited, and the potential for wormhole formation is reduced. Instead, the $CaCO_3$ at the edge of the MICP barrier in contact with the dissolution fluid may act as a sacrificial barrier which quickly buffers the dissolution fluid at the interface. Dissolution is therefore diffusion limited and the challenge lies not with the longevity of the $CaCO_3$, but with the initial delivery of bacteria and urea-$CaCl_2$ solution to the right locations so as to create a substantial low permeability seal.

Penetrability of bacteria is limited within this Berea sandstone. Whilst it could be improved beyond the observed 51 mm by reducing the concentration of bacteria injected (compensated for with an increased number of injection cycles) and increasing flow rate, it seems likely that it will remain low. Hence, MICP may be restricted to applications in the vicinity of the injection borehole.

$CaCO_3$ precipitation in this experiment took place under non-acidic conditions whereas, if bio-grouting were to be applied in an active carbon sequestration reservoir, the groundwater would be mildly acidic. To counteract the effect of mildly acidic conditions there are two options: 1) the reservoir fluid around the injection borehole could be displaced with non-acidic water of desired density and chemical composition, or 2) the pH of the urea-$CaCl_2$ solution (normally adjusted to 6.5 to delay the onset of precipitation) could be tailored to take into account mixing with the mildly acidic groundwater.

4.5. Implications for rock properties

The broader implications of this research may touch upon the natural formation and diagenesis of sandstones in which fluid flow has either deposited or removed cementing material. In such rocks, similar feedback between fluid flow and carbonate precipitation/dissolution, may be expected. Hence, their porosity may exhibit similar spatial correlation structures. Similar studies could illuminate the likely temporal evolution of pore structure in formations that undergo repeated cementation and dissolution events.

5. Conclusions

Microbially induced carbonate precipitation has been proposed as a bio-grout to greatly reduce the permeability of a sequestration reservoir host rock near the interface with the caprock as well as adjacent to boreholes. Due to the coupling of injection pathways with carbonate precipitation, preferential flow paths in the porous media are sealed first. This inhibits subsequent access to these pathways by acidic waters for dissolution, resulting in dissolution becoming diffusion limited. This, together with the buffering of the reservoir fluids by $CaCO_3$ dissolving at the periphery of the seal, results in the seal lasting far longer than would be predicted from a simple chemical equilibrium batch model. Provided that a high reduction in permeability was achieved over a substantial volume, MICP may prove to be a durable bio-grout for use in sequestration reservoirs, particularly for grouting the vicinity of injection wells.

The observed patterns of feedback between flow pathways, $CaCO_3$ precipitation, and dissolution may hold broader implications for spatial and temporal variation of pore structures in natural geological systems.

Acknowledgements

This work was funded by The Global Climate and Energy Project at Stanford University and the Engineering and Physical Sciences Research Council (EPSRC) Bright IDEAS award: The Big Pitch (grant number EP/M016854/1).

Appendix A. Supplementary data

Supplementary data associated with this article can be found, in the online version, at http://dx.doi.org/10.1016/j.ijggc.2017.07.007.

References

Ahrens, J., Berk, G., Law, C., 2005. ParaView: an end-user tool for large data visualization. Visualization Handbook. Elsevier.
Becker, M.W., Metge, D.W., Collins, S.A., Shapiro, A.M., Harvey, R.W., 2003. Bacterial transport experiments in fractured crystalline bedrock. Ground Water 41, 682–689.
Boever, E., De Varloteaux, C., Nader, F.H., Foubert, A., Békri, S., Youssef, S., Rosenberg, E., 2012. Quantification and prediction of the 3D pore network evolution in carbonate reservoir rocks. Oil Gas Sci. Technol. Rev. 67, 161–178. http://dx.doi.org/10.2516/ogst/2011170.
Cleveland Quarries, 2017. Berea Sandstone Petroleum Cores [WWW Document]. URL http://www.bereasandstonecores.com/, (Accessed 24 March 2017).
Cunningham, A.B., Phillips, A.J., Troyer, E., Lauchnor, E., Hiebert, R., Gerlach, R., Spangler, L., 2014. Wellbore leakage mitigation using engineered biomineralization. Energy Procedia 63, 4612–4619. http://dx.doi.org/10.1016/j.egypro.2014.11.494.
Dawson, G.K.W., Pearce, J.K., Biddle, D., Golding, S.D., 2015. Experimental mineral dissolution in Berea Sandstone reacted with CO2 or SO2-CO2 in NaCl brine under CO2 sequestration conditions. Chem. Geol. 399, 87–97. http://dx.doi.org/10.1016/j.chemgeo.2014.10.005.
de Marsily, G., 1986. Quantitative Hydrogeology, Groundwater Hydrogeology for Engineers, 1st ed. Academic Press, San Diego.
DeJong, J.T., Mortensen, B.M., Martinez, B.C., Nelson, D.C., 2010. Bio-mediated soil improvement. Ecol. Eng. 36, 197–210. http://dx.doi.org/10.1016/j.ecoleng.2008.12.029.
Dong, H., Rothmel, R., Onstott, T.C., Fuller, M.E., DeFlaun, M.F., Streger, S.H., Dunlap, R., Fletcher, M., 2002. Simultaneous transport of two bacterial strains in intact cores from Oyster, Virginia: biological effects and numerical modeling. Appl. Environ. Microbiol. 68, 2120–2132. http://dx.doi.org/10.1128/AEM.68.5.2120-2132.2002.
El Mountassir, G., Lunn, R.J., Moir, H., MacLachlan, E., 2014. Hydrodynamic coupling in microbially mediated fracture mineralization: formation of self-organized groundwater flow channels. Water Resour. Res. 50, 1–16. http://dx.doi.org/10.1002/2013WR013578.
Ellis, B.R., Fitts, J.P., Bromhal, G.S., McIntyre, D.L., Tappero, R., Peters, C.A., 2013. Dissolution-driven permeability reduction of a fractured carbonate caprock. Environ. Eng. Sci. 30, 187–193. http://dx.doi.org/10.1089/ees.2012.0337.
Ferris, F.G., Phoenix, V.R., Fujita, Y., Smith, R.W., 2003. Kinetics of calcite precipitation induced by ureolytic bacteria at 10–20 °C in artificial groundwater. Geochem. Cosmochim. Acta 67. http://dx.doi.org/10.1016/S0016-7037(00)00503-9.
Fujita, Y., Taylor, J.L., Gresham, T.L.T., Delwiche, M.E., Colwell, F.S., McLing, T.L., Petzke, L.M., Smith, R.W., 2008. Stimulation of microbial urea hydrolysis In groundwater to enhance calcite precipitation. Environ. Sci. Technol. 42, 3025–3032. http://dx.doi.org/10.1021/es702643g.
Gallagher, P.M., Spatari, S., Cucura, J., 2013. Hybrid life cycle assessment comparison of colloidal silica and cement grouted soil barrier remediation technologies. J. Hazard. Mater. 250–251, 421–430. http://dx.doi.org/10.1016/j.jhazmat.2013.01.065.
Handley-Sidhu, S., Sham, E., Cuthbert, M.O., Nougarol, S., Mantle, M., Johns, M.L., Macaskie, L.E., Renshaw, J.C., 2013. Kinetics of urease mediated calcite precipitation and permeability reduction of porous media evidenced by magnetic resonance imaging. Int. J. Environ. Sci. Technol. 10, 881–890. http://dx.doi.org/10.1007/s13762-013-0241-0.
Harbottle, M., Mugwar, A.J., Botusharova, S., 2016. Aspects of Implementation and Long-Term Performance of Biologically Induced Mineralisation of Carbonates in Porous Media. Goldschmidt 2016, Yokohama, Japan.
Iglauer, S., Sarmadivaleh, M., Al-Yaseri, A., Lebedev, M., 2014. Permeability evolution in sandstone due to injection of CO2-saturated brine or supercritical CO2 at reservoir conditions. Energy Procedia 63, 3051–3059. http://dx.doi.org/10.1016/j.egypro.2014.11.328.
Ivanov, V., Chu, J., 2008. Applications of microorganisms to geotechnical engineering for bioclogging and biocementation of soil in situ. Rev. Environ. Sci. Biotechnol. 7, 139–153. http://dx.doi.org/10.1007/s11157-007-9126-3.
Jonkers, H.M., Thijssen, A., Muyzer, G., Copuroglu, O., Schlangen, E., 2010. Application of bacteria as self-healing agent for the development of sustainable concrete. Ecol. Eng. 36, 230–235. http://dx.doi.org/10.1016/j.ecoleng.2008.12.036.
Krevor, S.C.M., Pini, R., Zuo, L., Benson, S.M., 2012. Relative permeability and trapping of CO2 and water in sandstone rocks at reservoir conditions. Water Resour. Res. 48. http://dx.doi.org/10.1029/2011WR010859.
Luquot, L., Gouze, P., 2009. Experimental determination of porosity and permeability changes induced by injection of CO2 into carbonate rocks. Chem. Geol. 265, 148–159. http://dx.doi.org/10.1016/j.chemgeo.2009.03.028.
Mangane, P.O., Gouze, P., Luquot, L., 2013. Permeability impairment of a limestone reservoir triggered by heterogeneous dissolution and particles migration during CO2-rich injection. Geophys. Res. Lett. 40, 4614–4619. http://dx.doi.org/10.1002/grl.50595.
Menke, H.P., Bijeljic, B., Andrew, M.G., Blunt, M.J., 2015. Dynamic three-dimensional pore-scale imaging of reaction in a carbonate at reservoir conditions. Environ. Sci.

Technol. 49, 4407–4414. http://dx.doi.org/10.1021/es505789f.
Minto, J.M., El Mountassir, E., Mountassir, G., Lunn, R.J., 2016. Rock fracture grouting with microbially induced carbonate precipitation. Water Resour. Res. 52, 8827–8844. http://dx.doi.org/10.1002/2016WR018884.
Mitchell, A.C., Ferris, F.G., 2005. The coprecipitation of Sr into calcite precipitates induced by bacterial ureolysis in artificial groundwater: temperature and kinetic dependence. Geochim. Cosmochim. Acta 69, 4199–4210. http://dx.doi.org/10.1016/j.gca.2005.03.014.
Mitchell, A.C., Phillips, A.J., Hiebert, R., Gerlach, R., Spangler, L.H., Cunningham, A.B., 2009. Biofilm enhanced geologic sequestration of supercritical CO2. Int. J. Greenh. Gas Control 3, 90–99. http://dx.doi.org/10.1016/j.ijggc.2008.05.002.
Mitchell, A.C., Phillips, A.J., Schultz, L.N., Parks, S.L., Spangler, L.H., Cunningham, A.B., Gerlach, R., 2013. Microbial CaCO3 mineral formation and stability in an experimentally simulated high pressure saline aquifer with supercritical CO2. Int. J. Greenh. Gas Control 15, 86–96. http://dx.doi.org/10.1016/j.ijggc.2013.02.001.
Mugwar, A.J., 2015. Bioprecipitation of Heavy Metals and Radionuclides with Calcium Carbonate in Aqueous Solutions and Particulate Media. Cardiff University.
Parkhurst, D.L., Appelo, C.A.J., 2013. Description of input and examples for PHREEQC version 3 – A computer program for speciation, batch- reaction, one-dimensional transport, and inverse geochemical calculations. U.S. Geological Survey Techniques and Methods. http://dx.doi.org/10.1016/0029-6554(94)90020-5. Book 6, Chapter A43.
Perrin, J.-C., Benson, S.M., 2010. An experimental study on the influence of sub-core scale heterogeneities on CO2 distribution in reservoir rocks. Transp. Porous Media 82, 93–109. http://dx.doi.org/10.1007/s11242-009-9426-x.
Phillips, A.J., Cunningham, A.B., Gerlach, R., Hiebert, R., Hwang, C., Lomans, B.P., Westrich, J., Mantilla, C., Kirksey, J., Esposito, R.A., Spangler, L., 2016. Fracture sealing with microbially-induced calcium carbonate precipitation: a field study. Environ. Sci. Technol.. http://dx.doi.org/10.1021/acs.est.5b05559. acs. est. 5b05559.
Pini, R., Krevor, S.C.M., Benson, S.M., 2012. Capillary pressure and heterogeneity for the CO2/water system in sandstone rocks at reservoir conditions. Adv. Water Resour. 38, 48–59. http://dx.doi.org/10.1016/j.advwatres.2011.12.007.
Schindelin, J., Rueden, C.T., Hiner, M.C., Eliceiri, K.W., 2015. The ImageJ ecosystem: an open platform for biomedical image analysis. Mol. Reprod. Dev. 82, 518–529. http://dx.doi.org/10.1002/mrd.22489.
Shaffer, G., 2010. Long-term effectiveness and consequences of carbon dioxide sequestration. Nat. Geosci. 3, 464–467. http://dx.doi.org/10.1038/ngeo896.
Sham, E., Mantle, M.D., Mitchell, J.K., Tobler, D.J., Phoenix, V.R., Johns, M.L., 2013. Monitoring bacterially induced calcite precipitation in porous media using magnetic resonance imaging and flow measurements. J. Contam. Hydrol. 152, 35–43. http://dx.doi.org/10.1016/j.jconhyd.2013.06.003.
Shell U.K. Limited, 2014. Peterhead CCS Project – Well Functional Specification (WFS) Document, Revision K02.
Sigfusson, B., Gislason, S.R., Matter, J.M., Stute, M., Gunnlaugsson, E., Gunnarsson, I., Aradottir, E.S., Sigurdardottir, H., Mesfin, K., Alfredsson, H.A., Wolff-Boenisch, D., Arnarsson, M.T., Oelkers, E.H., 2015. Solving the carbon-dioxide buoyancy challenge: the design and field testing of a dissolved CO2 injection system. Int. J. Greenh. Gas Control 37, 213–219. http://dx.doi.org/10.1016/j.ijggc.2015.02.022.
Suer, P., Hallberg, N., Carlsson, C., Bendz, D., Holm, G., 2009. Biogrouting compared to jet grouting: environmental (LCA) and economical assessment. J. Environ. Sci. Health. A. Tox. Hazard. Subst. Environ. Eng. 44, 346–353. http://dx.doi.org/10.1080/10934520802659679.
Tobler, D.J., Maclachlan, E., Phoenix, V.R., 2012. Microbially mediated plugging of porous media and the impact of differing injection strategies. Ecol. Eng. 42, 270–278. http://dx.doi.org/10.1016/j.ecoleng.2012.02.027.
Tobler, D.J., Cuthbert, M.O., Phoenix, V.R., 2014. Transport of Sporosarcina pasteurii in sandstone and its significance for subsurface engineering technologies. Appl. Geochem. 42, 38–44. http://dx.doi.org/10.1016/j.apgeochem.2014.01.004.
Tufenkji, N., 2007. Modeling microbial transport in porous media: traditional approaches and recent developments. Adv. Water Resour. 30, 1455–1469. http://dx.doi.org/10.1016/j.advwatres.2006.05.014.
van Paassen, L.A., 2009. Biogrout: Ground Improvement by Microbially Induced Carbonate Precipitation. Delft University of Technology.
Verba, C., Thurber, A.R., Alleau, Y., Koley, D., Colwell, F., Torres, M.E., 2016. Mineral changes in cement-sandstone matrices induced by biocementation. Int. J. Greenh. Gas Control 49, 312–322. http://dx.doi.org/10.1016/j.ijggc.2016.03.019.
Whiffin, V.S., van Paassen, L. a., Harkes, M.P., 2007. Microbial carbonate precipitation as a soil improvement technique. Geomicrobiol. J. 24, 417–423. http://dx.doi.org/10.1080/01490450701436505.
Woodward, J., 2005. An Introduction to Geotechnical Processes. CRC Press.